CLIMATOLOGY

Coral Sr/Ca-SST reconstruction from Fiji extending to ~1370 CE reveals insights into the Interdecadal Pacific Oscillation

Juan P. D'Olivo[1,2,3]*†, Jens Zinke[4,5,6]†, Rishav Goyal[7,8], Matthew H. England[8,9], Ariaan Purich[10], Thierry Corrège[11], Eduardo Zorita[12], Denis Scholz[13], Michael Weber[13], José D. Carriquiry[3]‡

The southwestern tropical Pacific is a key center for the Interdecadal Pacific Oscillation (IPO), which regulates global climate. This study introduces a groundbreaking 627-year coral Sr/Ca sea surface temperature reconstruction from Fiji, representing the IPO's southwestern pole. Merging this record with other Fiji and central tropical Pacific records, we reconstruct the SST gradient between the southwestern and central Pacific (SWCP), providing a reliable proxy for IPO variability from 1370 to 1997. This reconstruction reveals distinct centennial-scale temperature trends and insights into Pacific-wide climate impacts and teleconnections. Notably, the 20th century conditions, marked by simultaneous basin-scale warming and weak tropical Pacific zonal-meridional gradients, deviate from trends observed during the past six centuries. Combined with model simulations, our findings reveal that a weak SWCP gradient most markedly affects IPO-related rainfall patterns in the equatorial Pacific. Persistent synchronous western and central Pacific warming rates could lead to further drying climate across the Coral Sea region, adversely affecting Pacific Island nations.

INTRODUCTION

The Pacific Ocean is a major driver of climate variability, affecting human activities and natural ecosystems worldwide across timescales ranging from interannual to decadal and beyond (*1*–*3*). Tropical Pacific decadal variability (TPDV) plays a fundamental role in modulating the El Niño–Southern Oscillation (ENSO) (*4*–*7*), shifts in the intertropical and South Pacific convergence zones (ITCZ and SPCZ, respectively), and cyclogenesis in the western and southwestern Pacific islands (*4*). These changes have a strong impact on marine ecosystems, droughts, flooding rains, coral bleaching, and food availability both locally and remotely via atmospheric teleconnections (*8*, *9*).

This TPDV appears to be the result of low-frequency variations in ENSO and is strongly linked to the Interdecadal Pacific Oscillation (IPO) (*7*, *10*). The IPO reflects interdecadal fluctuations between warm and cold phases in the tropical eastern Pacific and opposite in sign subtropical sea surface temperature (SST) anomalies in the northwest and southwest Pacific (Fig. 1) (*7*, *11*). The IPO modulates Pacific and global climate patterns via its influence on the position and strength of the equatorial trade winds, which became clearly apparent during a period of relatively weak global warming between 1998 and 2013 (*12*), when strong trade winds kept a large fraction of the Pacific at colder than average temperatures. However, given the interdecadal nature of fluctuations in this phenomenon, the instrumental IPO record is too short to distinguish the influence of anthropogenic warming on its mean state. Climate model simulations show some skill in representing the spatial SST pattern of the IPO, but major deficiencies remain regarding the magnitude and extent of warming or cooling in the western Pacific (*7*). This hinders skillful prediction of global ENSO impacts modulated by Pacific decadal variability (*7*).

High-resolution paleoclimate records can extend the short instrumental record of the IPO and close the gap in our understanding of decadal climate variability. To date, paleoclimate reconstructions of the IPO over the past millennium have relied largely on records from far-field teleconnected regions on the fringes of the Pacific Ocean and other sites in the southwest Pacific (*13*–*15*). Currently, the oceanic IPO is limited to coral oxygen isotopes and Sr/Ca records from Fiji and the southwest Pacific starting in 1650 (*16*–*18*). Furthermore, current IPO reconstructions show limited agreement prior to the 20th century either due to nonstationary IPO relationships between geographical regions that are the basis of the reconstructions or to a lack of multicentennial oceanic IPO records or both. Therefore, a complete understanding of IPO variability is currently hindered by the limited availability of high-resolution continuous paleoclimate records from the southwest Pacific region, where SST variability is strongly linked to IPO variability. Long-lived corals from the southwest Pacific region are prime candidates to fill this oceanic IPO data gap. The coral Sr/Ca ratio serves as a robust direct geochemical proxy for the SST, capturing coral reef-scale and large-scale SST variability across the tropical oceans, while oxygen isotopes reflect a mixed signal of SST and salinity changes

[1]Unidad Académica de Sistemas Arrecifales, Instituto de Ciencias del Mar y Limnología, Universidad Nacional Autónoma de México, Puerto Morelos 77580, Mexico. [2]Institute for Geosciences, Freie Universität Berlin, Berlin 12249, Germany. [3]Instituto de Investigaciones Oceanológicas, Universidad Autónoma de Baja California, 22860 Ensenada, Baja California, Mexico. [4]School of Geology, Geography and Environment, University of Leicester, Leicester LE17RH, UK. [5]Molecular and Life Sciences, Curtin University, Perth, WA 6102, Australia. [6]Australian Institute of Marine Science, Townsville, QLD 4810, Australia. [7]Climate Change Research Centre, University of New South Wales, Sydney, NSW 2052, Australia. [8]ARC Centre for Excellence in Antarctic Science (ACEAS), University of New South Wales, Sydney, NSW 2052, Australia. [9]Centre for Marine Science and Innovation, University of New South Wales, Sydney, NSW 2052, Australia. [10]School of Earth, Atmosphere and Environment, and ARC Special Research Initiative for Securing Antarctica's Environmental Future, Monash University, Melbourne, VIC 3800, Australia. [11]EPOC, UMR 5805 CNR5, Université de Bordeaux, Pessac CEDEX F-33615, France. [12]Institute of Coastal Systems–Analysis and Modeling, Helmholtz Centre Hereon, Geesthacht 21502, Germany. [13]Institut für Geowissenschaften, Johannes Gutenberg-Universität Mainz, Mainz D-55128 Germany.
*Corresponding author. Email: dolivo@cmarl.unam.mx
†These authors contributed equally to this work.
‡Deceased.

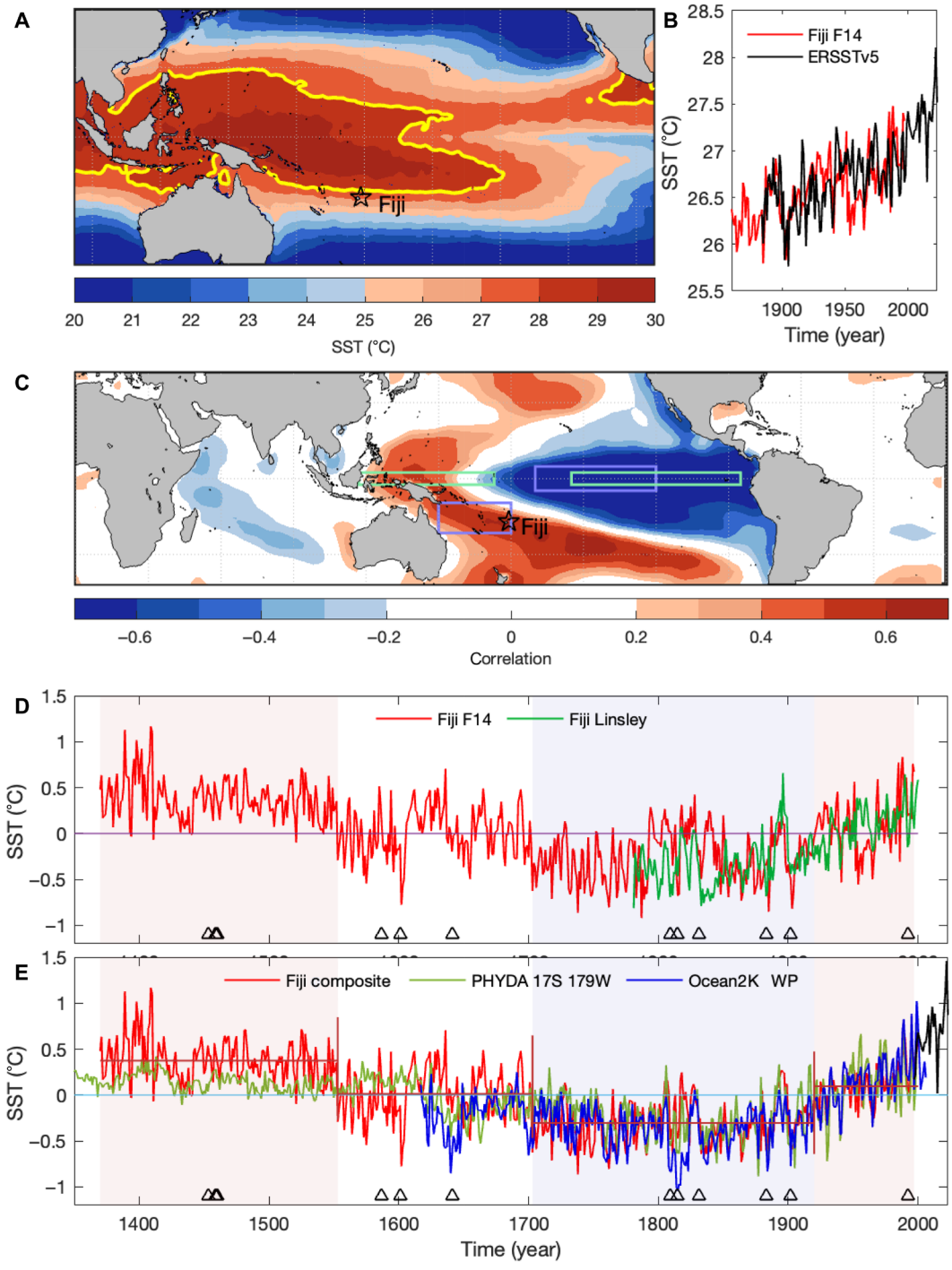

Fig. 1. Comparison of coral Sr/Ca-SST record with instrumental and reconstructed SST records. (**A**) ERSSTv5 average annual SST. The edge of the WPWP is indicated by the annual mean SST 28°C contour (yellow). (**B**) Annually averaged Sr/Ca-SSTs for coral core F14 from Fiji (red) compared to SSTs from ERSSTv5 (black) ($r = 0.39$, $P < 0.001$; 1883 to 1997). (**C**) Spatial correlation for the SWCP (purple rectangles) with the ERSSTv5 mean annual data. The green rectangles represent the zonal gradient of the SST between the western and eastern equatorial Pacific (*57*). (**D**) Annually averaged Sr/Ca-SSTs for coral core F14 from Fiji (red) compared to the Fiji composite coral record from records 1F and AB (*23*) (green) over their common period of 1781 to 1997. (**E**) Annual Fiji composite coral record (red) combining the records shown in (D) compared to the Ocean2K SST anomaly reconstruction for the western Pacific (*24*) (blue) and the SST from the PHYDA close to Fiji (17°S, 117°E) (*21*) (green). Also shown is the most recent SST data for Fiji from ERSSTv5 (1998 to 2021) shown in (E) (black). SST presented as anomalies relative to the period of 1883 to 1996. It should be noted that records 1F and AB (*23*) from Fiji are also included in the PHYDA and O2KWP reconstructions. Triangles in (D) and (E) denote the timing of major volcanic events (<−3.5 W/m^2 values) (Fig. 2) (*22*) typically associated with a cooling response. Extended warm (cold) periods highlighted in (D) and (E) by red (blue) bars based on the change point analysis for the Fiji composite shown in (E) are indicated by dark red vertical lines; dark red horizontal lines indicate the mean for each period.

(*19*). Consequently, the development of multicentennial coral Sr/Ca records is a prime target to reconstruct IPO-related SST variability, and this forms the primary focus of our present study.

The Fijian archipelago is located at the southern edge of the western Pacific Warm Pool (WPWP) and within the SPCZ, making it an ideal location to document the latitudinal expansion and contractions of the WPWP. This is important for quantifying the zonal and meridional SST gradients across the tropical and subtropical Pacific and is a crucial fingerprint of the IPO (Fig. 1). The IPO variability is spatially expressed as a horseshoe pattern of SST anomalies, in which the southwest and northwest subtropical Pacific anomalies show an opposite sign to the central and east Pacific anomalies (Fig. 1C). Average SST in these regions is used to define the strength of the IPO defined as the Tripole Index (*11*). The SST in the northwest Pacific pole is well correlated with the southwest Pacific pole. On the basis of this, the gradient between the southwest tropical Pacific and central equatorial Pacific (SWCP) should be a skillful proxy index for the IPO.

Here, we present an oceanic IPO index reconstruction that nearly doubles the length of previous reconstructions. This is made possible by generating a 627-year, ^{230}Th/U-dated, coral Sr/Ca record from Kanathea Island, a remote nearly deserted landmass situated within the Fijian Archipelago (17°14.93′S, 179°06.88′W), which represents the southwestern pole of the IPO (Fig. 1). This annually resolved *Diploastrea heliopora* record, designated F14, is the longest continuous coral Sr/Ca-SST reconstruction ever reported. We combine this record with existing paleoreconstructions from across the central tropical Pacific (*20*–*22*), along with climate model simulations, to develop a reconstruction of the SWCP gradient (Fig. 2). Our findings suggest that the latitudinal and longitudinal migrations of the WPWP are closely linked to the strength of the Pacific zonal-meridional temperature gradients, affecting ENSO and IPO spatial dynamics and climate teleconnections. Moreover, we demonstrate that the SST gradient between these regions in the SWCP is an effective tool for reconstructing the oceanic IPO variability for over six centuries. We show that a weak SWCP gradient or IPO has the most marked impacts on Pacific-wide rainfall and circulation patterns.

RESULTS

Unveiling centennial-scale southwest Pacific SST variability through Fiji coral records

Our SST reconstruction for Fiji is based on a composite record that combines our new long Sr/Ca coral record (F14; 1370 to 1997) with shorter, published Sr/Ca records (1781 to 1996) from the same region (*23*). This composite approach helps to reduce biases associated with using only one record and provides a more robust estimate of centennial-scale SST variability in the region. Our composite SST record is validated against instrumental data (Fig. 1A; $r = 0.56$, $P < 0.001$; 1883 to 1997) and demonstrates a high degree of correlation with reconstructed SSTs from other sources, including the Paleo Hydrodynamics Data Assimilation product (PHYDA) (*21*) and the large-scale Ocean 2K annual coral-SST reconstruction for the entire western Pacific and southeastern Indian Ocean (O2KWP) (Fig. 1E and table S5) (*24*). On a centennial timescale, a change point analysis of our SST reconstruction reveals four distinct periods in Fijian average temperatures over the past 627 years (Fig. 1E). Anomalously warm SST is observed between 1370 and 1553, followed by a transition period from 1553 to 1703. Colder conditions prevailed between 1703 and 1920, which includes the timing of the Little Ice Age, and then lastly an almost continuous warming trend from 1920 to 1997 at a rate of 0.46°C (±0.002°C, 95% confidence interval) per century. The high temperatures between 1370 and 1553 are only rivaled by instrumental SSTs recorded over the most recent 50 years (1973 to 2023), with temperatures after 2000 exceeding the 1370 to 1553 warm period and 2022 being the warmest year ever recorded in the Fiji region in the past 652 years.

We compared the Fiji composite data to simulate the SST from the Community Earth System Model (CESM1-CAM5) Last Millennium Ensemble (LME) to understand the origin of centennial variability in our reconstruction (Fig. 2A). Both our data and the LME show a long-term warming trend since the late 1800s, but the simulated SST anomalies are approximately one order of magnitude smaller than in our reconstruction. Over the 19th and 20th centuries, our Fiji coral reconstructed SST lies within ± 1 SD of the LME mean. However, between 1370 and 1553, our Fiji record and PHYDA (Fig. 2C) suggest much warmer SST conditions than those simulated by the CESM LME simulations. This relatively warm period is also found in low-resolution sedimentary archives from Indonesia in the core of the WPWP from Newton *et al.* (*25*) and Oppo *et al.* (*26*) (Fig. 2B). The resampled records (binned data of 10-year overlapping 50-year-long bins) show statistically significant correlations with our Fiji composite over the common period (1395 to 1825; $P < 0.001$, 95% confidence interval; $r = 0.70$ Fiji composite–Oppo; $r = 0.87$ Fiji composite–Newton; $r = 0.71$ Oppo-Newton; $n = 44$), indicating that the expansion or contraction of the WPWP recorded in Fiji proxy records is consistent with the general warming or cooling of the WPWP. The coherence between records from the WPWP and southwest tropical Pacific as well as the divergence from CESM LME simulations ensemble prior to 1553, suggesting that the impact of preindustrial external forcing (such as solar or volcanic activity) or the amplitude of internal Pacific variability (such as the dynamics of the WPWP) may not be well represented in these CESM simulations.

Although the two warmest periods observed in Fiji (1370 to 1553 and after 1920) are of similar magnitude, the records from the central and eastern Pacific indicate contrasting basin-scale spatial temperature patterns during these periods (Fig. 2, D to F). These differences likely reflect variations in the climate forcing and feedback mechanisms at work. The warm period observed in Fiji from the late 14th to mid-16th century appears to have been caused by a poleward expansion and warming of the WPWP most likely resulting from ocean-atmosphere dynamics (*27*). In contrast, warming since the late 19th century has been observed across much of the Pacific, except for the far eastern equatorial Pacific off South America, and is primarily driven by anthropogenic greenhouse forcing and trade wind responses (*28*, *29*).

Decoding the IPO through the SST gradient between the SWCP

In this study, we provide centennial information about the TPDV, and we test the hypothesis that the SST gradient between the SWCP can be used to reconstruct the oceanic IPO. To test this assumption, we first reconstructed the SWCP gradient between 1370 and 1995 using the Fiji composite record and central Pacific SST paleoclimate reconstructions (Fig. 2) (*21*, *30*). The reconstruction was validated against the instrumental SWCP gradient based on the Extended Reconstruction SSTs Version 5 (ERSSTv5) from 1883 to 1995 ($r = 0.71$; $P < 0.001$; fig. S8).

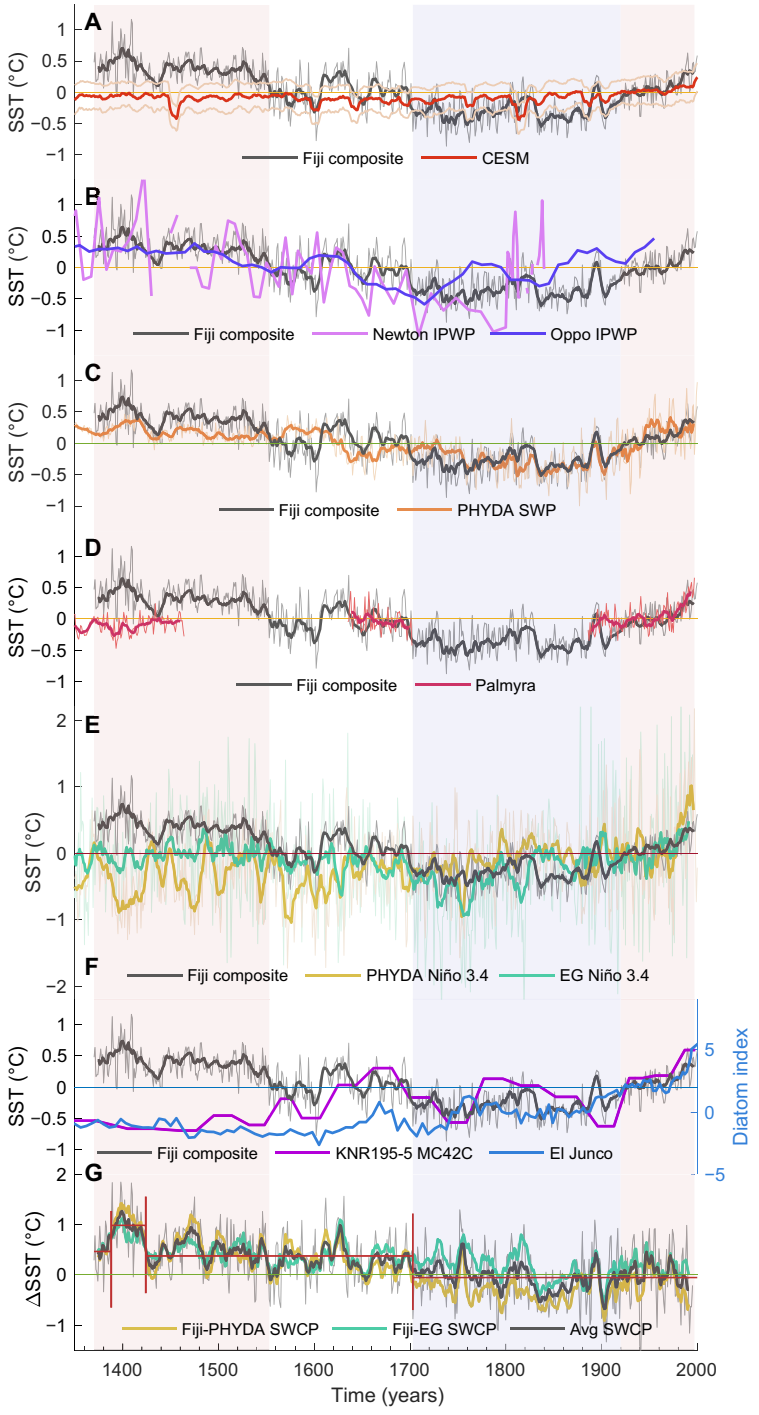

Fig. 2. Fiji coral composite annual Sr/Ca-SST record, WPWP model simulations and proxy reconstructions, and the SWCP SST gradient. Annual (light gray) and 15-year moving average (dark gray) Fiji coral composite record compared to (**A**) simulated southwest tropical Pacific (10° to 22°S, 150° to 180°E) SST based on the average of 13 runs from the CESM LME (red) and their SD (light red); (**B**) Makassar Strait composite Indo-Pacific Warm Pool SST Mg/Ca reconstructions from (*25*) (Newton, pink) and (*26*) (Oppo, purple); (**C**) annual and 15-year moving average SSTs reconstructed for the southwest tropical Pacific from the PHYDA (orange); (**D**) annual and 15-year moving average SST derived from $\delta^{18}O$ composite coral data from Palmyra (*60*); (**E**) annual and 15-year moving average SST reconstruction for the Niño 3.4 region in the central Pacific from (*21*) (PHYDA, yellow) and (*56*) (EG, green) based on the ERSSTv3; and (**F**) Mg/Ca foraminifera SST reconstruction from the Galapagos in the eastern Pacific (*61*) and inferred eastern Pacific SSTs from lake epiphytic diatom from El Junco Lake, Galápagos (*62*). (**G**) Annual and 15-year moving average SWCP gradient calculated as the difference between Fiji coral composite record and the Niño 3.4 SST reconstructions from the PHYDA (yellow) and EG (green) and their average (black). SST presented as anomalies relative to 1883 to 1996 except in (B) where values are relative to the common period between all three records (1370 to 1840). Extended warm (cold) periods in the Fiji composite highlighted in red (blue) based on the change point analysis from Fig. 1. Also shown in (G) is the change point analysis for the average SWCP gradient (dark red lines).

We contrasted our 627-year SWCP gradient reconstruction with the SWCP gradient inferred from the multivariate PHYDA dataset, which does not contain our coral record, and found an excellent agreement between the two ($r = 0.90$; $P < 0.001$; fig. S11). We also found that, between 1370 and 1553, the SST in Fiji diverged from the central Pacific, corresponding to the period of maximum strength in the SWCP gradient (Fig. 2, D to G, and fig. S12). From the 1700s, the SST in Fiji and the central Pacific converged and culminated in a near-synchronous warming trend in the SST in both regions observed over the most recent 120 years. The periods of basin-wide convergence between the southwestern and central Pacific records translated into a general weakening SWCP gradient, while the periods of divergence resulted in an enhanced SWCP gradient.

Despite synchronous warming across the tropical Pacific since the mid-19th century, we observe a moderate SWCP gradient strengthening compared with the early 19th century when the gradient was at its minimum (Fig. 2G). While this strengthening is not statistically significant, it agrees with a reported strengthening of the zonal gradient and Pacific Walker Circulation in recent decades (*28*, *31*). Our findings, based on reconstructions and observations, contrast Coupled Model Intercomparison Project Phase 6 (CMIP6)–based multimodel mean (MMM) simulations and some other observational estimates of zonal gradient trends during the current warm period, which suggest a general weakening of the zonal gradient and Walker Circulation with increasing greenhouse gas forcing (*32*, *33*). This mismatch between observations and the simulations suggests that either a considerable footprint of internal long-term Pacific climate variability is present in the observations or the simulations do not accurately reflect the forced climate response to increasing greenhouse gases (*34*). Nevertheless, our reconstruction reveals that, despite a weak recent upturn in the SWCP gradient, the gradient is far weaker than between the 14th and 16th centuries.

To assess if the TPDV obtained from our SWCP gradient reconstruction accurately captures the IPO variability, we compare it with instrumental SST data (Fig. 3A). This comparison reveals a notable spatial correlation between the reconstructed SWCP gradient and SST across the Pacific, closely mirroring the IPO pattern. Our IPO reconstruction exhibits highly significant agreement with instrumental IPO data from 1880 onward ($r = 0.85$, $P \leq 0.0001$; 1880 to 1995). Notably, this correlation is stronger than for other recent long-term IPO reconstructions ($r = 0.54$, $P \leq 0.0001$; 1880 to 1995) based on far-field ice core reconstructions (1450 to 1996) (*14*), underscoring the uncertainty in reconstructing the IPO based on remote land-based teleconnections.

The reconstruction of the SWCP gradient reveals a centennial component in the expression of the IPO, frequency, and magnitude over 1370 to 1995 (Fig. 3C). During the Little Ice Age (LIA), a prolonged positive expression of the IPO is observed, coinciding with a minimum in the centennial variability of the gradient. The magnitude of the wavelet power spectrum highlights the 1400s as a period with the strongest expression of multidecadal (10 to 50 years) variability within the six-century span covered by our reconstruction. This period aligns with the time when the SWCP gradient reached its maximum strength between 1370 and 1995, hinting at a possible relationship between the gradient's magnitude and the expression of the IPO. Ideally, this relationship should be confirmed based on longer reconstructions covering periods with different strengths of the SWCP gradient.

We next investigate the impacts of the strength of the SWCP gradient, a footprint for the IPO, on the spatial patterns of the SST and precipitation and sea level pressure anomalies related to the SPCZ over centennial scales. To do this, we calculated the gradient using preindustrial control simulations obtained from multiple CMIP6 models to obtain composites that show the strength and sign of the gradient corresponding to distinct spatial patterns for the SST, rainfall, and sea level pressure for the Indo-Pacific region (Fig. 4 and fig. S13). While coupled climate models have deficiencies in their representation of some features of tropical climate (*7*), they remain important tools to analyze covarying spatial patterns of climate variables over timescales beyond the recent observational period. The CMIP6 MMM composites demonstrate that the strength, sign, and spatial patterns of the IPO can be defined by SST variability in the SWCP (Fig. 4), highlighting the importance of our reconstruction as the longest continuous record of SST variability in the southwest Pacific. This enables us to understand local and remote teleconnections resulting from past IPO variability.

This spatial analysis shows that the magnitude of the SWCP gradient is an important factor for the mean state and teleconnections in the Indo-Pacific region. A weaker gradient is associated with larger SST anomalies and precipitation changes across the equatorial Pacific (Fig. 4, C and D). In addition, these conditions correspond to weak extratropical anomalies as well as stronger mean sea level pressure (MSLP) changes in the extratropical region of both hemispheres (Fig. 4, C and D, and fig. S13). The expression of the SPCZ appears to be particularly sensitive to the state of the SWCP in both its orientation and magnitude (Fig. 4), with the diagonal orientation and variability of the SPCZ being the result of tropical and extratropical atmospheric interactions and the SST conditions. In the CMIP6 MMM composites, when the SWCP gradient is strong and has a positive (negative) sign as observed prior to the 1700s in our reconstruction, this translates to enhanced (reduced) rainfall in the southwestern Pacific including the Fiji region and Coral Sea with drying (wetting) to the east of Fiji (Fig. 4, A and B). When the SCWP is weak and either positive or negative (<0.1 SD), the expression of the SPCZ becomes displaced zonally and eastward with pronounced drying over the Fiji region stretching across the Coral Sea. The latter are the conditions observed during the most recent period of anthropogenic warming since the late 19th century (weakly positive SWCP).

To validate our predictions, we compared the gradient reconstruction with seawater $\delta^{18}O$ for the WPWP (*26*), a hydrological proxy (fig. S14). On the basis of the CMIP6 MMM composites in Fig. 4 (E to H), when the gradient is weak (regardless of the sign), rainfall is high, indicated by more negative seawater $\delta^{18}O$ in the western Pacific. A strongly positive gradient (>1) corresponds to weakly positive rainfall, while a strongly negative gradient (<−1) corresponds to negative rainfall. The wettest period in the hydrological reconstructions, spanning the 1600s to 1700s, coincides with an extended weak gradient and the overall lowest mean SST in the western and southwestern Pacific. During the mid-1800s, when the gradient turns weakly negative, rainfall remains positive. Conversely, rainfall appears to weaken during the late 1300s to early 1400s, corresponding to a stronger gradient and higher mean SSTs in the western and southwestern Pacific. This comparison lends confidence to the predictions from the CMIP6 MMM composites. However, further work is needed. Specifically, expanding the number and length of current paleohydrological reconstructions in the tropical oceans is crucial.

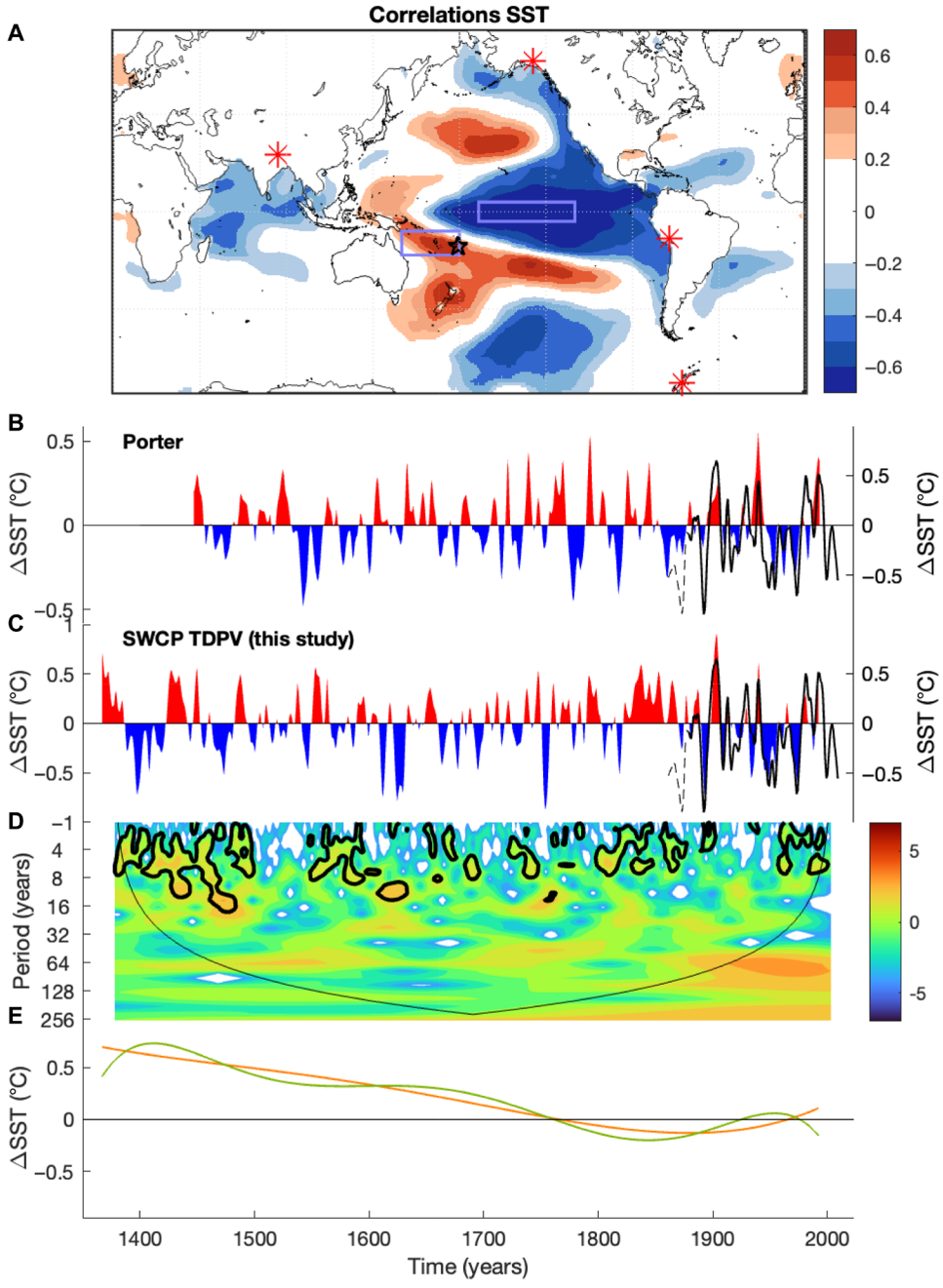

Fig. 3. IPO reconstruction. (**A**) Spatial correlation for the reconstructed annual SWCP SST gradient with the ERSSTv5 mean annual data. Red asterisks highlight the location of the ice core records used in previous reconstructions (*14*), the purple rectangles denote the area used to define the SWCP gradient, and the black star denotes the location of Fiji. (**B**) Porter's IPO reconstruction based on the ice core records (*14*) and (**C**) this study's IPO reconstruction based on the TPDV obtained from the SWCP SST gradient (colored area plot). In (B) and (C), IPO reconstructions are compared to the instrumental IPO data (black line) [IPO data available at the National Oceanic and Atmospheric Administration (NOAA)] (*11*). The period prior to 1880 is shown by a discontinuous line to highlight the decrease in confidence in instrumental data (see Materials and Methods). (**D**) Wavelet power spectrum for the SWCP SST gradient (*63*). The shaded contours are the normalized variance where warm colors indicate a higher power. The thin line is the "cone of influence" highlighting potential edge effects, and the bold line contours are the >95% confidence interval for a lag −1 of 0.72 for a red noise background (bold line). (**E**) Long-term (centennial) variability for the SWCP gradient based on a fourth-degree (orange) and sixth-degree (green) polynomial fit.

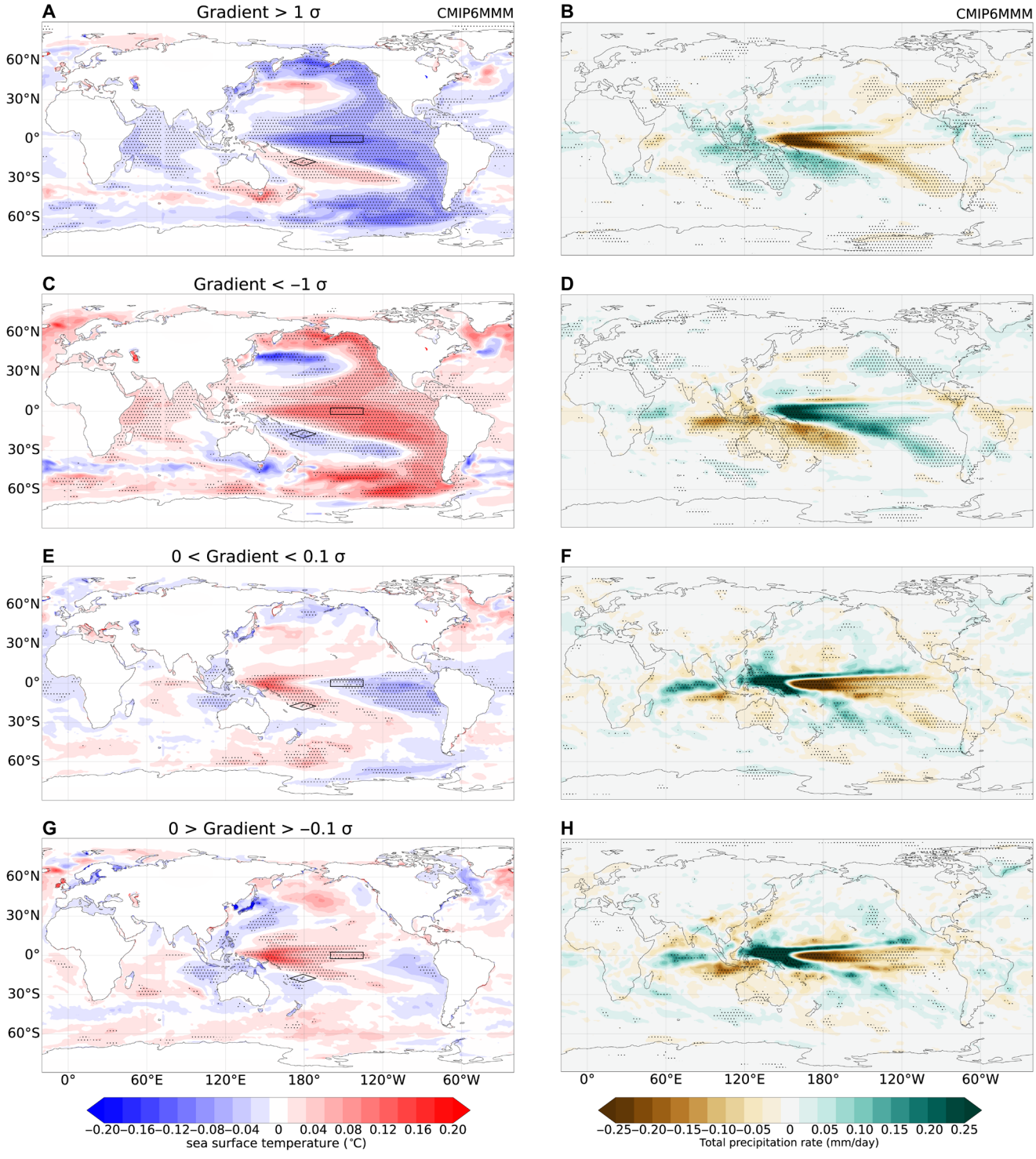

Fig. 4. Composite maps of simulated SST (left) and precipitation (right). (**A** to **H**) In each case, four different regimes are included based on the magnitude of the SWCP gradient calculated using data from 16,062 years of the CMIP6 preindustrial control simulation. (A) and (B) represent composites obtained when there is a strong positive SWCP gradient (i.e., warmer temperature over Fiji compared to central Pacific and the magnitude of the gradient is >1 SD), and (C) and (D) represent a strong inverse SWCP gradient (i.e., warmer temperature in the central Pacific than in Fiji and the SWCP gradient is <−1 SD). The bottom two rows represent composites when the SWCP gradient is weaker (less than 0.1 SD), with (E) and (F) showing composite maps when the gradient is weak and positive and (G) and (H) representing composites when the gradient is weak and negative. Stripling on the plots represents significant values at 95% significance level using a two-tailed *t* test. Composites from each model are computed first before calculating the MMM composite to provide equal weightage to each CMIP6 model used in the study.

DISCUSSION

Our study unveils an unprecedented 627-year independently dated coral record from Fiji and develops a reconstruction of the SWCP temperature gradient, providing valuable insights into the multidecadal to century-scale variability in the Pacific. The reconstruction of the SWCP gradient indicates that the 20th century conditions of concurrent Pacific basin-scale warming, and weak tropical Pacific temperature gradients are atypical for the past six centuries. Furthermore, the TPDV derived from our reconstructed SWCP gradient is shown to reflect the IPO SST pattern, allowing us to extend the oceanic IPO index to an unprecedented 627 years. When coupled with simulation data, our reconstruction shows that, during the transition periods when the SWCP gradient is weak, there is a less regular expression of the IPO, and it is during these periods that the SST and precipitation in the western tropical Pacific show some of the strongest anomalies. The Pacific-wide impacts of the IPO on the SST and rainfall, as well as the resulting far-reaching teleconnections, appear to depend on the centennial mean state of the SWCP gradient. Our six-century-long reconstruction revealed that the similarly paced current anthropogenic warming in the central and southwestern Pacific since the late 19th century has reversed the SWCP gradient reconstructed for previous centuries, albeit weakly. This is associated with stronger interdecadal IPO and SPCZ swings. There is evidence that the SWCP strengthened from a strongly negative state in the 1800s to a weakly negative state in the 1900s in line with the shift toward positive IPO. This translated to marked dampening at the heart of the WPWP and drying toward the central and eastern Pacific. The question remains as to how ongoing global warming and predicted Pacific Walker Circulation weakening may reinforce those IPO swings toward further drying during the remainder of the 21st century with potentially adverse effects for the inhabitants of vulnerable Pacific Islands and their ecosystems.

MATERIALS AND METHODS

Coral core collection and sampling

During the Paleofiji cruise in July 1998 by the IRD (France), a 2.6-m continuous coral core (F14) was collected at 17°14.93′S, 179°06.88′W near Kanathea, in the Fijian archipelago. The 2.6-m core was collected with a hydraulic drill from the top of a living *D. heliopora* massive coral growing at a 3-m depth below the surface. The coral colony was found on an exterior reef plain, with sand substrate and surrounded by coral patches dominated by tubular and branched acroporides, and some favides. Core sections were cut into ~1.1-cm-thick slabs along the major axis of growth. Slabs were rinsed in deionized water, cleaned with an ultrasonic probe, and oven-dried at 45°C. X-ray radiography images of the slabs revealed clear regular annual density bands (fig. S1). A Delta 8″ drill press with a 2.4-mm bit was used to recover coral powder for geochemical analysis. This coral species presents large (~1 cm in diameter) corallites with distinctive columella and septa structures (*35*). This gives the opportunity to select the coral structure during the milling of powder samples used in geochemical analyses. Damassa *et al.* (*35*) and Watanabe *et al.* (*36*) suggested the use of a columella material, while Bagnato *et al.* (*37*) argued that robust results could be obtained from either columella or septal structures. In this study, the columella skeletal material was sampled continuously along the axis of maximum growth at 1-mm intervals, generating 2250 samples.

Despite careful sampling of the coral core, it is possible that some samples included small contributions from other skeletal structures due to the complexity of the skeleton. These contributions are, however, likely to be small and random in nature and therefore add no systematic long-term variability to the data, which is the focus of this study. Potential sampling issues are described in more detail in the Supplementary Materials. X-ray diffraction (XRD) analysis (X'Pert, Phillips) was performed on skeletal samples at selected intervals; no evidence of diagenetic alteration of the coral skeleton was identified in the core.

Geochemical analysis of Sr/Ca

Analysis of Sr/Ca was carried on all samples to generate records of the past SST. To eliminate possible contamination from organic matter and metal adsorption, each sample underwent a rigorous cleaning procedure modified from (*38*). This cleaning process consisted of three sequential-cumulative steps. First, 1 ml of ultrapure H_2O (18.2 microhms) was added to the sample and left in an ultrasonic bath for 15 min at ambient temperature. Then, 0.25 ml of 30% ultrapure H_2O_2 was added to the sample and left in an ultrasonic bath for 15 min at 60°C. Last, 1 ml of ultrapure 4 mM HNO_3 was added to the samples and put in the ultrasonic bath for 15 min at atmospheric temperature. Samples were centrifuged for 4 min between each step, and the supernatant liquid was carefully removed by siphoning with a micropipette.

Before analysis, 1 mg of cleaned coral powder from each sample was dissolved in 5 ml of 2 M ultrapure HNO_3. Strontium and calcium were simultaneously measured in all samples using a Thermo Jarrell Ash, model Iris AP, inductively coupled plasma optical emission spectrometer (ICP-OES) at the Instituto de Investigaciones Oceanológicas of the Universidad Autónoma de Baja California, in Ensenada, Mexico. The sample analysis was performed following the intensity ratio calibration method described by de Villiers *et al.* (*39*). A set of calibration solutions (SPEX) with constant Ca values and variable Sr was gravimetrically prepared with concentrations covering ranges typical of coral skeletal material. For every five samples, a calibration standard was analyzed to correct for drift, and for every nine samples, a laboratory-prepared coral standard was analyzed to estimate the precision. The overall external precision obtained for the Sr/Ca from the coral standard was 0.028 mmol/mol (1 σ). Following this methodology, Villaescusa and Carriquiry (*40*) obtained a precision of ±0.28% (1 σ) for Sr/Ca in *Porites* sp. and *Pavona* sp. corals. The precision for Sr/Ca of this study was ±0.31% (1 σ).

Core chronology

The chronology for the core was based on multiple counting of the annual density bands from positive and negative x-ray radiograph images by two people (fig. S1) supported by skeletal Sr/Ca annual cycles. Chronology peak matching of the geochemical signal was performed with the AnalySeries software (*41*). For the geochemical data, the Sr/Ca most recent value was tied with its corresponding SST value, then extremes of each annual cycle between series were tied using "peak to peak" matching. Both chronology methods yield similar results with an overall age of 627 years and a linear extension rate of ~3.6 mm/year. This age model was confirmed by ^{230}Th/U dating (next section), yielding undistinguishable age differences between methods when considering ±2 years uncertainties in each method.

The 1-mm sample resolution generated approximately four samples per year, in general, sufficient to identify annual cycles in the

series (fig. S2). This resolution does not, however, allow us to resolve the full resolution of the seasonal variability particularly in the years when skeletal growth was reduced; in such cases, the information was obtained solely from the growth bands. The coral Sr/Ca record was resampled to annual resolution using the built-in linear interpolation function in the AnalySeries software (*41*). The annual record spanned from 1370 to 1997 as the 1998 band was still in formation at the time when the core was collected and thus excluded. The chronology was cross-checked with volcanic events (*42*) (Fig. 1D) and with known El Niño events (*43*) recompilation. These events were used as an initial guide for tie points, but the final chronology was adjusted in AnalySeries based on the seasonal information from the Sr/Ca and not constricted by these reference points.

U-Th dating

A small piece from the bottom of the offcut adjacent to the slab used for the geochemical analyses was cut and dated using the ^{230}Th/U method at the Institute for Geosciences, Johannes Gutenberg-University Mainz, Germany (table S1). The coral subsample of ~250 mg was prepared by column chemistry and analyzed by multicollector ICP mass spectrometry (MC-ICPMS; Neptune Plus). The weighed sample was briefly leached in 7 N HNO_3 to remove potential surface contamination and dissolved in 7 N HNO_3, and a mixed ^{229}Th-^{233}U-^{236}U spike was added [see (*44*) for details on spike calibration]. Potential organic material was removed by adding a mixture of concentrated HNO_3, HCl, and H_2O_2. The dried sample was then dissolved in 6 N HCl, and U and Th were separated using ion-exchange column chemistry (*45*). Details about the MC-ICPMS procedures are described in (*46*). All activity ratios were calculated using the decay constants as shown in (*47*) and corrected for detrital contamination assuming a ^{232}Th/^{238}U weight ratio of 3.8 for the detritus and ^{230}Th, ^{234}U, and ^{238}U in secular equilibrium. The correction is not significant within error.

On the basis of the x-ray data, this piece is estimated to have been located ~14 years below the last sample collected for geochemical analysis, which corresponds to approximately AD 1356. The ^{230}Th/U method yielded a date of AD 1359.5 ± 2.0 years, which aligns excellently with an uncertainty of ±2 years for the age model based on band counting and geochemical data.

SST calculations from Sr/Ca

The instrumental annual (January to December) SST from the ERSSTv5 (*48*) database for the 2° × 2° grid centered at 18°S, 180°W (the region that includes Fiji) was used to convert the coral Sr/Ca record to temperature values. The ERSSTv5 product was used instead of HADISST as it showed a slightly better agreement (higher correlations) with the coral data (fig. S3 and table S2). The ERSSTv5 record shows a good agreement with the higher resolution but shorter (1982 onward) OISSTv2 1° × 1° SST product grid centered at 17.5°S, 179.5°W ($r = 0.946$, $P < 0.001$) (*49*).

Figure S3 shows the good agreement between the annual ERSSTv5 SST data and the annual Sr/Ca record during the period of 1883 to 1997 ($r = -0.361$, $P < 0.001$). The congruence between the series improved during the past 20 years (1978 to 1997; $r = -0.528$, $P < 0.001$), like the relationship between the Sr/Ca reconstruction and OISSTv2 (1982 to 1997; $r = -0.546$, $P = 0.028$). This is expected as the quality of instrumental data markedly reduces with time. The latter is especially true in the southern tropical Pacific as data prior to the 1970s are very scarce (*50*, *51*). Before 1883, the instrumental data deviated from our Sr/Ca record; this was also observed in other coral records in the region (*23*), suggesting a critical decay in the quality of the instrumental database. Therefore, the instrumental data from the ERSSTv5 before 1883 were excluded from all calculations.

The coral Sr/Ca data were converted to temperature data by scaling the coral data to match the average and SD of the ERSSTv5 over the 1883 to 1997 period. As a first approach, different linear regression calibrations for different periods were tested; however, as indicated by the root mean square error (RMSE) calculated for the period of 1883 to 1997 (table S3), better results were obtained when the Sr/Ca-SST data were scaled to match the average and variability of the instrumental record. Scaling annual Sr/Ca records to generate SST reconstructions with more realistic amplitude has been used to improve calibrations from annual data (*23*, *52*). Here, the data were scaled in a two-step process. First, the SST and Sr/Ca records were normalized using standard scores to the calibration period of the most recent 110 years (1883 to 1997) according to

$$n\mathrm{Sr/Ca}_i = \left(\mathrm{Sr/Ca}_i - m\mathrm{Sr/Ca}\right)/\sigma\mathrm{Sr/Ca}$$

$$n\mathrm{SST}_i = \left(\mathrm{SST}_i - m\mathrm{SST}\right)/\sigma\mathrm{SST}$$

Then, we used the SD and mean from the ERSSTv5 to convert the standardized Sr/Ca record to temperature values

$$\mathrm{SSTSr/Ca} = n\mathrm{Sr/Ca}_i \times \sigma\mathrm{SST} + m\mathrm{SST}$$

where σSST and σSr/Ca are the SD over 1883 to 1997 for the SST instrumental record and for the coral Sr/Ca data, respectively. *m*SST and *m*Sr/Ca are the mean over 1883 to 1997 for the SST instrumental record and for the coral Sr/Ca record, respectively. SST_i and $\mathrm{Sr/Ca}_i$ are the SST and Sr/Ca parameters at certain points in time, respectively. Second, the Sr/Ca was converted to SST (SSTSr/Ca) values using the instrumental record's mean and SD values over the selected period (1883 to 1997). The improvements from scaling the data compared to a traditional calibration (e.g., using a linear regression between the coral and SST data) were evident in reducing the RMSE observed in table S3.

Selecting the appropriate calibration period/method also has important implications in the quantitative analysis of the temperature reconstructions (fig. S4), for example, in the estimation of the magnitude of warming or cooling but not on the overall trends. This can be clearly observed when different calibration periods are selected to calibrate the F14 Sr/Ca record against the same instrumental record. In the case of our record, we observed that the best reconstructions were obtained for the 1978 to 1997 period and for the scaled data. All other calibration periods amplified the temperature changes, which, for example, resulted in an overestimation of the warming over the past 113 years (1883 to 1997). We observed that scaling the coral data, in general, produced data that best matched the warming of 0.52°C recorded by the instrumental ERSSTv5 data over the period of 1883 to 1997 (table S4). Scaling the data reduced some of the effects on the temperature calibrations from periods when the correlation of the Sr/Ca data with the SST was reduced, which masked the real sensitivity of the proxy to temperature changes. In this sense, when the relationship between Sr/Ca and the SST is expressed as a linear equation of the form $\mathrm{Sr/Ca} = m * \mathrm{SST} + c$, the noise in the data reduces the "real" sensitivity (m) of the Sr/Ca to temperature; however, when solved for $\mathrm{SST} = (\mathrm{Sr/Ca} - c)/m$, this error ends up overestimating the temperature variability as observed in fig. S4.

Composite SST record

The Sr/Ca record from core F14 was significantly correlated with other Sr/Ca records from Fiji (cores AB and 1F) (*23*). Correlations between our core F14 with core AB (excluding anomalous data prior to 1725; $r = 0.35$, $P < 0.001$, $n = 272$) and with core 1F ($r = 0.34$, $P < 0.001$, $n = 215$) were like the correlations between cores AB and 1F ($r = 0.40$, $P < 0.001$, $n = 215$). Despite the overall good agreement on a longer timescale during some periods, there were differences at the interannual level between all three cores (fig. S5). Uncertainties in the records due to sampling, analytical errors, vital effects, or local variability could explain some of these differences (see the Supplementary Materials). We created a composite record including information from all three records to reduce these effects. The composite record included the data from our 627-year record (F14) and the 215 years of overlap (1781 to 1996) from cores 1F and AB. We limited the interpretation of this combined data to general assertions about long-term changes and avoided discussing specific brief events. Our SST reconstruction alone (core F14) showed significant correlations with reconstructed SSTs for Fiji from the PHYDA ($r = 0.47$ F14-PHYDA, $P < 0.001$; 1370 to 1996) (*21*) and the O2KWP ($r = 0.37$, $P < 0.001$; 1617 to 1997) (*24*). Combining our Fiji record with the existing coral Sr/Ca data from Fiji (1781 to 1996) (*23*) into a composite record (Fiji composite) improved the correlation with the ERSSTv5 ($r = 0.57$, $P < 0.001$; 1883 to 1997; Fig. 1E) and the PHYDA data from Fiji ($r = 0.55$, $P < 0.001$; 1370 to 1996) and the O2KWP ($r = 0.49$, $P < 0.001$, $n = 381$; 1617 to 1997), an improved correlation is expected, although the Fiji records in (*23*) are included in the PHYDA and O2KWP reconstructions.

Modeled SST data

The simulations analyzed in this study were conducted with the state-of-the art CESM version 1.1 with Community Atmosphere Model version 5 (CESM1-CAM5). CESM is a coupled earth system model comprising atmosphere, ocean, and sea-ice modules and is driven by estimations of external climate forcing, including solar output, volcanic eruptions, greenhouse trace gases, and land-use changes, as described below.

The CESM LME used for this study consists of 13 "all-forcings" runs (three runs added at a later stage) all branched from the same date chosen at random from the preindustrial control run (fig. S6). The initial atmospheric conditions were numerically perturbed 13 times to obtain the initial conditions for each simulation in the LME. These CESM simulations are not part of the CMIP; however, CESM is a successor of CCSM4, which participated in CMIP5.

The past millennium simulations are conducted with prescribed atmospheric concentrations of carbon dioxide and methane. As described above, the initial conditions for these simulations are chosen at random from control preindustrial simulations—the actual initial conditions are unknown. This means that the timing of internal climate variability, such as ENSO and the IPO, is not synchronized with real-world internal climate variations. Within the simulation ensemble, each individual simulation represents an a priori equally probable evolution of the climate conditioned by the imposed external forcing. A detailed description of the past millennium forcings used in the CESM simulations is provided elsewhere (*53*). We also extracted the SWCP gradient from past millennium simulations performed with CMIP5 models MPI-ESM (*54*) and CCSM4 (*55*) (fig. S6). For more details on the models, see the Supplementary Materials.

Gradient calculation

We defined SWCP as the difference between the box in the southwest tropical Pacific (10° to 22°S, 150° to 180°E) including Fiji and the Niño 3.4 region (5°N-S, 190° to 240°E). To extend the SWCP prior to the instrumental record, we calculated the difference between the coral composite record from Fiji and the SST reconstructions for the Niño 3.4 region from (*56*) (EG-N3.4) and (*21*) (PHYDA) (fig. S7). The EG-N3.4 anomalies were calibrated back to absolute temperatures using the ERSSTv5 data for the area covering Niño 3.4 over the period of 1883 to 1995. Comparisons of the mean SWCP paleoreconstruction with instrumental SST-derived records of the SWCP and zonal gradient (defined as the difference between 2.5°N-S, 117° to 173°E and 2.5°N-S, 205° to 275°E) (*57*) since the late-19th century validate our reconstruction of the SWCP and indicate a relationship to the zonal gradient (fig. S8, A and B). We find that our SWCP paleoreconstruction is highly correlated with estimates of the gradients based on instrumental ERSSTv5 ($r = 0.77$ zonal gradient; $r = 0.83$ SWCP; $P < 0.001$; 1883 to 1995). Running correlations of 31 years attest to the stability of these relationships since the 1880s (fig. S8). Spatial correlations for the reconstructed SWCP SST gradient with the SST indicate an ENSO-like pattern across the Pacific and teleconnections to the Indian Ocean (fig. S8C). These spatial SST correlations from the coral-based index (Fig. 3 and fig. S9) are a mirror image of those for the zonal gradient and SWCP instrumental data (Fig. 1 and fig. S10). We further validated our reconstruction by calculating the gradient from our Fiji composite and the coral annual Sr/Ca record from Palmyra (figs. S7 and S9) (*58*), which lies in the area of influence of Niño 3.4, obtaining similar results as with the average SWCP from EG-N3.4 and PHYDA ($r = 0.59$ zonal gradient and $r = 0.67$ SWCP, $P < 0.001$; 1883 to 1995). The link between the WPWP and the eastern Pacific predicts a relationship between the SWCP and the zonal gradient, which is confirmed by instrumental reconstructions for the SWCP and zonal gradient ($r = 0.97$, $P < 0.001$; 1883 to 1997).

IPO reconstruction

To reconstruct the IPO, we used the TPDV derived from our reconstructed SWCP gradient, which includes the SWCP nodes considered in the definition for the IPO proposed by Henley *et al.* (*11*). On the basis of this definition and the characteristic horseshoe pattern of the IPO, we assume that the southwest and northwest poles mirror each other. To extract the TPDV component from the SWCP gradient and reconstruct the IPO, we detrended the SWCP using a second-degree polynomial and applied a Chebyshev Type I filter [as proposed by Henley *et al.* (*11*) with a second-order lowpass with 0.5 dB of peak-to-peak ripple in the passband and a passband-edge frequency of 0.125].

One limitation of using the TPDV derived from the SCWP gradient as a proxy for the IPO is that it only incorporates data from the equatorial and southern nodes of the IPO. Obtaining data from the northern node would help validate the findings of this study and further establish the prevalence of the IPO as the dominant mode of variability during the past centuries-millennia.

CMIP6 data

Monthly averaged MSLP, precipitation, and SST data from preindustrial control simulations of 23 CMIP6 models (total 16,062 years of data) were used in this study to generate composite maps based

on the magnitude of the SWCP gradient (Fig. 4 and fig. S13). CMIP6 models used and the number of years analyzed are shown in table S6.

Statistical analysis

Statistical significance in all running and spatial correlations were computed against a 1000-sample Monte Carlo (*59*). 95% significance levels were calculated and illustrated for running correlations and colored in all spatial correlation maps. Running correlations and spatial correlations were calculated in KNMI Climate Explorer (*59*) and later redrawn with MATLAB. Abrupt changes in the mean of records were calculated using MATLAB's change point analysis with the maximum number of changes limited to three. The Chebyshev filter was applied using the MATLAB built-in function cheby1.

Supplementary Materials

This PDF file includes:

Supplementary Text
Figs. S1 to S15
Tables S1 to S6
References

REFERENCES AND NOTES

1. A. Timmermann, S. I. An, J. S. Kug, F. F. Jin, W. J. Cai, A. Capotondi, K. M. Cobb, M. Lengaigne, M. J. McPhaden, M. F. Stuecker, K. Stein, A. T. Wittenberg, K. S. Yun, T. Bayr, H. C. Chen, Y. Chikamoto, B. Dewitte, D. Dommenget, P. Grothe, E. Guilyardi, Y. G. Ham, M. Hayashi, S. Ineson, D. Kang, S. Kim, W. Kim, J. Y. Lee, T. Li, J. J. Luo, S. McGregor, Y. Planton, S. Power, H. Rashid, H. L. Ren, A. Santoso, K. Takahashi, A. Todd, G. M. Wang, G. J. Wang, R. H. Xie, W. H. Yang, S. W. Yeh, J. Yoon, E. Zeller, X. B. Zhang, El Niño-Southern Oscillation complexity. *Nature* **559**, 535–545 (2018).
2. A. Santoso, M. J. Mcphaden, W. J. Cai, The defining characteristics of ENSO extremes and the strong 2015/2016 El Niño. *Rev. Geophys.* **55**, 1079–1129 (2017).
3. W. J. Cai, L. X. Wu, M. Lengaigne, T. Li, S. McGregor, J. S. Kug, J. Y. Yu, M. F. Stuecker, A. Santoso, X. C. Li, Y. G. Ham, Y. Chikamoto, B. Ng, M. J. McPhaden, Y. Du, D. Dommenget, F. Jia, J. B. Kajtar, N. Keenlyside, X. P. Lin, J. J. Luo, M. Martin-Rey, Y. Ruprich-Robert, G. J. Wang, S. P. Xie, Y. Yang, S. M. Kang, J. Y. Choi, B. L. Gan, G. I. Kim, C. E. Kim, S. Kim, J. H. Kim, P. Chang, Pantropical climate interactions. *Science* **363**, eaav4236 (2019).
4. W. J. Cai, M. Lengaigne, S. Borlace, M. Collins, T. Cowan, M. J. McPhaden, A. Timmermann, S. Power, J. Brown, C. Menkes, A. Ngari, E. M. Vincent, M. J. Widlansky, More extreme swings of the South Pacific convergence zone due to greenhouse warming. *Nature* **488**, 365–369 (2012).
5. W. Q. Han, G. A. Meehl, A. X. Hu, J. Zheng, J. Kenigson, J. Vialard, B. Rajagopalan, Yanto, Decadal variability of the Indian and Pacific Walker cells since the 1960s: Do they covary on decadal time scales? *J. Clim.* **30**, 8447–8468 (2017).
6. H. Heidemann, T. Cowan, S. B. Power, B. J. Henley, Statistical relationships between the Interdecadal Pacific Oscillation and El Niño-Southern Oscillation. *Clim. Dyn.* **188**, 114634 (2023).
7. S. Power, M. Lengaigne, A. Capotondi, M. Khodri, J. Vialard, B. Jebri, E. Guilyardi, S. McGregor, J. S. Kug, M. Newman, M. J. McPhaden, G. Meehl, D. Smith, J. Cole, J. Emile-Geay, D. Vimont, A. T. Wittenberg, M. Collins, G. I. Kim, W. J. Cai, Y. Okumura, C. Chung, K. M. Cobb, F. Delage, Y. Y. Planton, A. Levine, F. Zhu, J. Sprintall, E. Di Lorenzo, X. B. Zhang, J. J. Luo, X. P. Lin, M. Balmaseda, G. J. Wang, B. J. Henley, Decadal climate variability in the tropical Pacific: Characteristics, causes, predictability, and prospects. *Science* **374**, eaay9165 (2021).
8. J. R. Brown, M. Lengaigne, B. R. Lintner, M. J. Widlansky, K. van der Wiel, C. Dutheil, B. K. Linsley, A. J. Matthews, J. Renwick, South Pacific Convergence Zone dynamics, variability and impacts in a changing climate. *Nat. Rev. Earth Environ.* **1**, 530–543 (2020).
9. R. V. Rohli, G. A. Snedden, E. R. Martin, K. L. DeLong, Impacts of ocean-atmosphere teleconnection patterns on the south-central United States. *Front. Earth Sci.* **10**, 934654 (2022).
10. A. Capotondi, S. McGregor, M. J. McPhaden, S. Cravatte, N. J. Holbrook, Y. Imada, S. C. Sanchez, J. Sprintall, M. F. Stuecker, C. C. Ummenhofer, M. Zeller, R. Farneti, G. Graffino, S. J. Hu, K. B. Karnauskas, Y. Kosaka, F. Kucharski, M. Mayer, B. Qiu, A. Santoso, A. S. Taschetto, F. Wang, X. B. Zhang, R. M. Holmes, J. J. Luo, N. Maher, C. Martinez-Villalobos, G. A. Meehl, R. Naha, N. Schneider, S. Stevenson, A. Sullivan, P. van Rensch, T. T. Xu, Mechanisms of tropical Pacific decadal variability. *Nat. Rev. Earth Environ.* **4**, 754–769 (2023).
11. B. J. Henley, J. Gergis, D. J. Karoly, S. Power, J. Kennedy, C. K. Folland, A tripole index for the interdecadal Pacific oscillation. *Clim. Dyn.* **45**, 3077–3090 (2015).
12. M. H. England, S. McGregor, P. Spence, G. A. Meehl, A. Timmermann, W. J. Cai, A. Sen Gupta, M. J. McPhaden, A. Purich, A. Santoso, Recent intensification of wind-driven circulation in the Pacific and the ongoing warming hiatus. *Nat. Clim. Chang.* **4**, 222–227 (2014).
13. B. K. Linsley, P. P. Zhang, A. Kaplan, S. S. Howe, G. M. Wellington, Interdecadal-decadal climate variability from multicoral oxygen isotope records in the South Pacific Convergence Zone region since 1650 A.D. *Paleoceanography* **23**, 5139 (2008).
14. S. E. Porter, E. Mosley-Thompson, L. G. Thompson, A. B. Wilson, Reconstructing an interdecadal Pacific oscillation index from a Pacific basin-wide collection of ice core records. *J. Clim.* **34**, 3839–3852 (2021).
15. B. M. Buckley, C. C. Ummenhofer, R. D. D'Arrigo, K. G. Hansen, L. H. Truong, C. N. Le, D. K. Stahle, Interdecadal Pacific Oscillation reconstructed from trans-Pacific tree rings: 1350-2004 CE. *Clim. Dyn.* **53**, 3181–3196 (2019).
16. K. L. DeLong, T. M. Quinn, F. W. Taylor, C.-C. Shen, K. Lin, Improving coral-base paleoclimate reconstructions by replicating 350 years of coral Sr/Ca variations. *Palaeogeogr. Palaeoclimatol. Palaeoecol.* **373**, 6–24 (2013).
17. N. Tangri, R. B. Dunbar, B. K. Linsley, D. M. Mucciarone, ENSO's shrinking twentieth-century footprint revealed in a half-millennium coral core from the South Pacific Convergence Zone. *Palaeogeogr. Palaeoclimatol.* **33**, 1136–1150 (2018).
18. B. K. Linsley, H. C. Wu, E. P. Dassié, D. P. Schrag, Decadal changes in South Pacific sea surface temperatures and the relationship to the Pacific decadal oscillation and upper ocean heat content. *Geophys. Res. Lett.* **42**, 2358–2366 (2015).
19. D. M. Thompson, Environmental records from coral skeletons: A decade of novel insights and innovation. *Wiley Interdiscip. Rev. Clim.* **13**, 745 (2022).
20. M. L. Griffiths, A. K. Kimbrough, M. K. Gagan, R. N. Drysdale, J. E. Cole, K. R. Johnson, J. X. Zhao, B. I. Cook, J. C. Hellstrom, W. S. Hantoro, Western Pacific hydroclimate linked to global climate variability over the past two millennia. *Nat. Commun.* **7**, 11719 (2016).
21. N. J. Steiger, J. E. Smerdon, E. R. Cook, B. I. Cook, A reconstruction of global hydroclimate and dynamical variables over the Common Era. *Sci. Data* **5**, 180086 (2018).
22. T. J. Crowley, Causes of climate change over the past 1000 years. *Science* **289**, 270–277 (2000).
23. B. K. Linsley, A. Kaplan, Y. Gouriou, J. Salinger, P. B. deMenocal, G. M. Wellington, S. S. Howe, Tracking the extent of the South Pacific convergence zone since the early 1600s. *Geochem. Geophys. Geosyst.* **7**, 1115 (2006).
24. J. E. Tierney, N. J. Abram, K. J. Anchukaitis, M. N. Evans, C. Giry, K. H. Kilbourne, C. P. Saenger, H. C. Wu, J. Zinke, Tropical sea surface temperatures for the past four centuries reconstructed from coral archives. *Paleoceanography* **30**, 226–252 (2015).
25. A. Newton, R. Thunell, L. Stott, Climate and hydrographic variability in the Indo-Pacific Warm Pool during the last millennium. *Geophys. Res. Lett.* **33**, 27234 (2006).
26. D. W. Oppo, Y. Rosenthal, B. K. Linsley, 2,000-year-long temperature and hydrology reconstructions from the Indo-Pacific warm pool. *Nature* **460**, 1113–1116 (2009).
27. A. C. Clement, R. Seager, M. A. Cane, S. E. Zebiak, An ocean dynamical thermostat. *J. Clim.* **9**, 2190–2196 (1996).
28. R. Seager, M. Cane, N. Henderson, D. E. Lee, R. Abernathey, H. H. Zhang, Strengthening tropical Pacific zonal sea surface temperature gradient consistent with rising greenhouse gases. *Nat. Clim. Chang.* **9**, 517–522 (2019).
29. J. Liu, B. Wang, M. A. Cane, S. Y. Yim, J. Y. Lee, Divergent global precipitation changes induced by natural versus anthropogenic forcing. *Nature* **493**, 656–659 (2013).
30. J. Emile-Geay, K. M. Cobb, M. E. Mann, A. T. Wittenberg, Estimating central equatorial Pacific SST variability over the past millennium. Part I: Methodology and validation. *J. Clim.* **26**, 2302–2328 (2013).
31. E. S. Chung, A. Timmermann, B. J. Soden, K. J. Ha, L. Shi, V. O. John, Reconciling opposing walker circulation trends in observations and model projections. *Nat. Clim. Chang.* **9**, 405–412 (2019).
32. R. Seager, N. Henderson, M. Cane, Persistent discrepancies between observed and modeled trends in the tropical Pacific Ocean. *J. Clim.* **35**, 4571–4584 (2022).
33. W. J. Cai, A. Santoso, M. Collins, B. Dewitte, C. Karamperidou, J. S. Kug, M. Lengaigne, M. J. McPhaden, M. F. Stuecker, A. S. Taschetto, A. Timmermann, L. X. Wu, S. W. Yeh, G. J. Wang, B. Ng, F. Jia, Y. Yang, J. Ying, X. T. Zheng, T. Bayr, J. R. Brown, A. Capotondi, K. M. Cobb, B. L. Gan, T. Geng, Y. G. Ham, F. F. Jin, H. S. Jo, X. C. Li, X. P. Lin, S. McGregor, J. H. Park, K. Stein, K. Yang, L. Zhang, W. X. Zhong, Changing El Niño–Southern Oscillation in a warming climate. *Nat. Rev. Earth Environ.* **2**, 628–644 (2021).
34. S. Lee, M. L'Heureux, A. T. Wittenberg, R. Seager, P. A. O'Gorman, N. C. Johnson, On the future zonal contrasts of equatorial Pacific climate: Perspectives from observations, simulations, and theories. *NPJ Clim. Atmos. Sci.* **5**, 82 (2022).
35. T. D. Damassa, J. E. Cole, H. R. Barnett, T. R. Ault, T. R. McClanahan, Enhanced multidecadal climate variability in the seventeenth century from coral isotope records in the western Indian Ocean. *Paleoceanography* **21**, 1217 (2006).
36. T. Watanabe, A. Juillet-Leclerc, J. P. Cuif, C. Rollion-Bard, Y. Dauphin, S. Reynaud, Recent advances in coral biomineralization with implications for paleo-climatology: A brief overview. *Elsevier Oceanogr. Ser.* **73**, 239–254 (2007).

37. S. Bagnato, B. K. Linsley, S. S. Howe, G. M. Wellington, J. Salinger, Evaluating the use of the massive coral *Diploastrea heliopora* for paleoclimate reconstruction. *Paleoceanography* **19**, 935 (2004).
38. T. Mitsuguchi, T. Uchida, E. Matsumoto, P. J. Isdale, T. Kawana, Variations in Mg/Ca, Na/Ca, and Sr/Ca ratios of coral skeletons with chemical treatments: Implications for carbonate geochemistry. *Geochim. Cosmochim. Acta* **65**, 2865–2874 (2001).
39. S. de Villiers, M. Greaves, H. Elderfield, An intensity ratio calibration method for the accurate determination of Mg/Ca and Sr/Ca of marine carbonates by ICP-AES. *Geochem. Geophys. Geosyst.* **3**, n/a-n/a (2002).
40. J. A. Villaescusa, J. D. Carriquiry, Calibration of Sr/Ca and Mg/Ca paleothermometers in coral Porites sp. from San Benedicto Island, Revillagigedo Archipelago, Mexico. *Cienc. Mar.* **30**, 603–618 (2004).
41. D. Paillard, L. Labeyrie, P. Yiou, Macintosh program performs time-series analysis. *Eos* **77**, 379–379 (1996).
42. T. J. Crowley, T. M. Quinn, F. W. Taylor, C. Henin, P. Joannot, Evidence for a volcanic cooling signal in a 335-year coral record from New Caledonia. *Paleoceanography* **12**, 633–639 (1997).
43. W. H. Quinn, V. T. Neal, "The historical record of El Niño events" in *Climate Since A.D. 1500* (Routledge, 1992).
44. L. Gibert, G. R. Scott, D. Scholz, A. Budsky, C. Ferrandez, F. Ribot, R. A. Martin, M. Leria, Chronology for the Cueva Victoria fossil site (SE Spain): Evidence for early Pleistocene Afro-Iberian dispersals. *J. Hum. Evol.* **90**, 183–197 (2016).
45. Q. C. Yang, D. Scholz, K. P. Jochum, D. L. Hoffmann, B. Stoll, U. Weis, B. Schwager, M. O. Andreae, Lead isotope variability in speleothems—A promising new proxy for hydrological change? First results from a stalagmite from western Germany. *Chem. Geol.* **396**, 143–151 (2015).
46. J. C. Obert, D. Scholz, T. Felis, W. M. Brocas, K. P. Jochum, M. O. Andreae, 230Th/U dating of Last Interglacial brain corals from Bonaire (southern Caribbean) using bulk and theca wall material. *Geochim. Cosmochim. Acta* **178**, 20–40 (2016).
47. H. Cheng, R. L. Edwards, C. C. Shen, V. J. Polyak, Y. Asmerom, J. Woodhead, J. Hellstrom, Y. J. Wang, X. G. Kong, C. Spotl, X. F. Wang, E. C. Alexander, Improvements in ^{230}Th dating, ^{230}Th and ^{234}U half-life values, and U-Th isotopic measurements by multi-collector inductively coupled plasma mass spectrometry. *Earth Planet. Sci. Lett.* **371–372**, 82–91 (2013).
48. B. Y. Huang, P. W. Thorne, V. F. Banzon, T. Boyer, G. Chepurin, J. H. Lawrimore, M. J. Menne, T. M. Smith, R. S. Vose, H. M. Zhang, Extended reconstructed sea surface temperature, version 5 (ERSSTv5): Upgrades, validations, and intercomparisons. *J. Clim.* **30**, 8179–8205 (2017).
49. R. W. Reynolds, N. A. Rayner, T. M. Smith, D. C. Stokes, W. Q. Wang, An improved in situ and satellite SST analysis for climate. *J. Clim.* **15**, 1609–1625 (2002).
50. N. A. Rayner, Global analyses of sea surface temperature, sea ice, and night marine air temperature since the late nineteenth century. *J. Geophys. Res.* **108**, 2670 (2003).
51. A. Kaplan, M. A. Cane, Y. Kushnir, A. C. Clement, M. B. Blumenthal, B. Rajagopalan, Analyses of global sea surface temperature 1856–1991. *J. Geophys. Res.* **103**, 18567–18589 (1998).
52. J. Zinke, A. Hoell, J. M. Lough, M. Feng, A. J. Kuret, H. Clarke, V. Ricca, K. Rankenburg, M. T. McCulloch, Coral record of southeast Indian Ocean marine heatwaves with intensified Western Pacific temperature gradient. *Nat. Commun.* **6**, 8562 (2015).
53. B. L. Otto-Bliesner, E. C. Brady, J. Fasullo, A. Jahn, L. Landrum, S. Stevenson, N. Rosenbloom, A. Mai, G. Strand, Climate variability and change since 850 CE: An ensemble approach with the Community Earth System Model. *Bull. Am. Meteorol. Soc.* **97**, 735–754 (2016).
54. J. H. Jungclaus, K. Lohmann, D. Zanchettin, Enhanced 20th-century heat transfer to the Arctic simulated in the context of climate variations over the last millennium. *Clim. Past* **10**, 2201–2213 (2014).
55. L. Landrum, B. L. Otto-Bliesner, E. R. Wahl, A. Conley, P. J. Lawrence, N. Rosenbloom, H. Y. Teng, Last millennium climate and its variability in CCSM4. *J. Clim.* **26**, 1085–1111 (2013).
56. J. Emile-Geay, K. M. Cobb, M. E. Mann, A. T. Wittenberg, Estimating central equatorial Pacific SST variability over the past millennium. Part II: Reconstructions and implications. *J. Clim.* **26**, 2329–2352 (2013).
57. S. Coats, K. B. Karnauskas, Are simulated and observed twentieth century tropical Pacific sea surface temperature trends significant relative to internal variability? *Geophys. Res. Lett.* **44**, 9928–9937 (2017).
58. I. S. Nurhati, K. M. Cobb, E. Di Lorenzo, Decadal-scale SST and salinity variations in the central tropical Pacific: Signatures of natural and anthropogenic climate change. *J. Clim.* **24**, 3294–3308 (2011).
59. V. Trouet, G. J. Van Oldenborgh, KNMI Climate Explorer: A web-based research tool for high-resolution paleoclimatology. *Tree-Ring Res.* **69**, 3–13 (2013).
60. S. G. Dee, K. M. Cobb, J. Emile-Geay, T. R. Ault, R. L. Edwards, H. Cheng, C. D. Charles, No consistent ENSO response to volcanic forcing over the last millennium. *Science* **367**, 1477–1481 (2020).
61. G. T. Rustic, A. Koutavas, T. M. Marchitto, B. K. Linsley, Dynamical excitation of the tropical Pacific Ocean and ENSO variability by Little Ice Age cooling. *Science* **350**, 1537–1541 (2015).
62. J. L. Conroy, A. Restrepo, J. T. Overpeck, M. Steinitz-Kannan, J. E. Cole, M. B. Bush, P. A. Colinvaux, Unprecedented recent warming of surface temperatures in the eastern tropical Pacific Ocean. *Nat. Geosci.* **2**, 46–50 (2009).
63. C. Torrence, G. P. Compo, A practical guide to wavelet analysis. *Bull. Am. Meteorol. Soc.* **79**, 61–78 (1998).
64. J. M. Lough, Coral calcification from skeletal records revisited. *Mar. Ecol. Prog. Ser.* **373**, 257–264 (2008).
65. T. Mitsuguchi, E. Matsumoto, T. Uchida, Mg/Ca and Sr/Ca ratios of *Porites* coral skeleton: Evaluation of the effect of skeletal growth rate. *Coral Reefs* **22**, 381–388 (2003).
66. S. de Villiers, G. T. Shen, B. K. Nelson, The SrCa-temperature-temperature relationship in coralline aragonite: Influence of variability in $(SrCa)_{seawater}$ and skeletal growth parameters. *Geochim. Cosmochim. Acta* **58**, 197–208 (1994).
67. C. Alibert, M. T. McCulloch, Strontium/calcium ratios in modern *porites* corals from the Great Barrier Reef as a proxy for sea surface temperature: Calibration of the thermometer and monitoring of ENSO. *Paleoceanography* **12**, 345–363 (1997).
68. R. Rashid, A. Eisenhauer, V. Liebetrau, J. Fietzke, F. Bohm, M. Wall, S. Krause, A. Ruggeberg, W. C. Dullo, H. Jurikova, E. Samankassou, B. Lazar, Early diagenetic imprint on temperature proxies in holocene corals: A case study from French Polynesia. *Front. Earth Sci.* **8**, 301 (2020).
69. A. Ribaud-Laurenti, B. Hamelin, L. Montaggioni, D. Cardinal, Diagenesis and its impact on Sr/Ca ratio in Holocene *Acropora* corals. *Int. J. Earth Sci.* **90**, 438–451 (2001).
70. A. Müller, M. K. Gagan, M. T. McCulloch, Early marine diagenesis in corals and geochemical consequences for paleoceanographic reconstructions. *Geophys. Res. Lett.* **28**, 4471–4474 (2001).
71. N. Griffiths, W. Muller, K. G. Johnson, O. A. Aguilera, Evaluation of the effect of diagenetic cements on element/Ca ratios in aragonitic Early Miocene (~16 Ma) Caribbean corals: Implications for 'deep-time' palaeo-environmental reconstructions. *Palaeogeogr. Palaeoclimatol. Palaeoecol.* **369**, 185–200 (2013).
72. E. J. Hendy, M. K. Gagan, J. M. Lough, M. McCulloch, P. B. deMenocal, Impact of skeletal dissolution and secondary aragonite on trace element and isotopic climate proxies in *Porites* corals. *Paleoceanography* **22**, 1462 (2007).
73. N. Allison, A. Finch, J. Webster, D. Clague, Palaeoenvironmental records from fossil corals: The effects of submarine diagenesis on temperature and climate estimates. *Geochim. Cosmochim. Acta* **71**, 4693–4703 (2007).
74. S. de Villiers, B. K. Nelson, A. R. Chivas, Biological controls on coral Sr/Ca and δ18O reconstructions of sea surface temperatures. *Science* **269**, 1247–1249 (1995).
75. R. M. Walter, H. R. Sayani, T. Felis, K. M. Cobb, N. J. Abram, A. K. Arzey, A. R. Atwood, L. D. Brenner, E. P. Dassie, K. L. DeLong, B. Ellis, J. Emile-Geay, M. J. Fischer, N. F. Goodkin, J. A. Hargreaves, K. H. Kilbourne, H. Krawczyk, N. P. McKay, A. L. Moore, S. A. Murty, M. R. Ong, R. D. Ramos, E. V. Reed, D. Samanta, S. C. Sanchez, J. Zinke, The CoralHydro2k Database: A global, actively curated compilation of coral δ18O and Sr/Ca proxy records of tropical ocean hydrology and temperature for the Common Era. *Earth Syst. Sci. Data* **15**, 2081–2116 (2023).
76. J. P. D'Olivo, D. J. Sinclair, K. Rankenburg, M. T. McCulloch, A universal multi-trace element calibration for reconstructing sea surface temperatures from long-lived Porites corals: Removing 'vital-effects'. *Geochim. Cosmochim. Acta* **239**, 109–135 (2018).
77. P. Montagna, M. McCulloch, E. Douville, M. L. Correa, J. Trotter, R. Rodolfo-Metalpa, D. Dissard, C. Ferrier-Pagès, N. Frank, A. Freiwald, S. Goldstein, C. Mazzoli, S. Reynaud, A. Rüggeberg, S. Russo, M. Taviani, Li/Mg systematics in scleractinian corals: Calibration of the thermometer. *Geochim. Cosmochim. Acta* **132**, 288–310 (2014).
78. T. M. DeCarlo, G. A. Gaetani, A. L. Cohen, G. L. Foster, A. E. Alpert, J. A. Stewart, Coral Sr-U thermometry. *Paleoceanography* **31**, 626–638 (2016).
79. K. M. Cobb, C. D. Charles, H. Cheng, R. L. Edwards, El Niño/Southern Oscillation and tropical Pacific climate during the last millennium. *Nature* **424**, 271–276 (2003).
80. H. R. Sayani, K. M. Cobb, K. DeLong, N. T. Hitt, E. R. M. Druffel, Intercolony δ18O and Sr/Ca variability among *Porites* spp. corals at Palmyra Atoll: Toward more robust coral-based estimates of climate. *Geochem. Geophys. Geosyst.* **20**, 5270–5284 (2019).
81. M. K. Gorman, T. M. Quinn, F. W. Taylor, J. W. Partin, G. Cabioch, J. A. Austin, B. Pelletier, V. Ballu, C. Maes, S. Saustrup, A coral-based reconstruction of sea surface salinity at Sabine Bank, Vanuatu from 1842 to 2007 CE. *Paleoceanography* **27**, PA3226 (2012).
82. T. M. Quinn, T. J. Crowley, F. W. Taylor, New stable isotope results from a 173-year coral from Espiritu Santo, Vanuatu. *Geophys. Res. Lett.* **23**, 3413–3416 (1996).
83. T. M. Quinn, F. W. Taylor, SST artifacts in coral proxy records produced by early marine diagenesis in a modern coral from Rabaul, Papua New Guinea. *Geophys. Res. Lett.* **33**, (2006).
84. H. C. Wu, B. K. Linsley, E. P. Dassié, B. Schiraldi, P. B. deMenocal, Oceanographic variability in the South Pacific Convergence Zone region over the last 210 years from multi-site coral Sr/Ca records. *Geochem. Geophys. Geosyst.* **14**, 1435–1453 (2013).

85. B. K. Linsley, G. M. Wellington, D. P. Schrag, Decadal sea surface temperature variability in the subtropical South Pacific from 1726 to 1997 A.D. *Science* **290**, 1145–1148 (2000).
86. Y. Kawakubo, C. Alibert, Y. Yokoyama, A reconstruction of subtropical western North Pacific SST variability back to 1578, based on a *Porites* Coral Sr/Ca record from the Northern Ryukyus, Japan. *Paleoceanography* **32**, 1352–1370 (2017).
87. T. P. Guilderson, D. P. Schrag, Reliability of coral isotope records from the western Pacific warm pool: A comparison using age-optimized records. *Paleoceanography* **14**, 457–464 (1999).
88. C. D. Charles, K. Cobb, M. D. Moore, R. G. Fairbanks, Monsoon–tropical ocean interaction in a network of coral records spanning the 20th century. *Mar. Geol.* **201**, 207–222 (2003).
89. M. C. Osborne, R. B. Dunbar, D. A. Mucciarone, E. Druffel, J.-A. Sanchez-Cabeza, A 215-yr coral δ18O time series from Palau records dynamics of the West Pacific Warm Pool following the end of the Little Ice Age. *Coral Reefs* **33**, 719–731 (2014).

Acknowledgments: L'Institut de Recherche pour le Développement (IRD), France, is greatly thanked for providing the samples and sponsoring a Visiting Professor Fellowship (DSF Bourse) for J.D.C. to Noumea, New Caledonia. We thank J. Villaescusa, G. Horta-Puga, R. Mertz, and P. G. Castro-Castro for valuable support in the laboratories. We thank M. Avalos from UNAM for providing the XRD analysis. We are also grateful for the insightful comments and suggestions of S. Eggins and K. Cobb to previous versions of the manuscript. We acknowledge the World Climate Research Programme's Working Group on Coupled Modeling, which is responsible for CMIP, and thank the climate modeling groups for producing and making their model output available. We dedicate this manuscript to J.D.C., who passed away in mid-2023.
Funding: Funding support for this study was provided by CONACYT (Mexico) PN (2018/no. 2916) and UABC to J.D.C. Funding for field logistics during collection of the coral core in Fiji was provided by the IRD; a Royal Society Wolfson Fellowship supported J.Z. (RSWF_FT_180000). A.P. is supported by the Australian Research Council Special Research Initiative for Securing Antarctica's Environmental Future (SR200100005). M.H.E. and R.G. are supported by the ARC Centre for Excellence in Antarctic Science (ARC grant SR200100008). We thank the Instituto de Ciencias del Mar y Limnología, UNAM, for contributions toward publication costs. **Author contributions:** J.D.C. conceived the study with T.C. (who collected the core). J.D.C. supervised the coral sample preparation (slabbing, x-raying, and microdrilling), and J.P.D. conducted the chemical preparation and analyzed the samples by ICP-OES. E.Z. provided the simulated CESM southwest tropical Pacific temporal data. R.G. analyzed the CMIP6 preindustrial control simulation and provided corresponding spatial patterns. D.S. and M.W. performed ^{230}Th/U dating of the coral. J.D.C. supervised the project. J.P.D. and J.Z. took the lead in interpreting the data and writing the manuscript. All authors substantially contributed with the interpretation of the data as well as the writing and editing of the manuscript. **Competing interests:** The authors declare that they have no competing interests. **Data and materials availability:** All data needed to evaluate the conclusions in the paper are present in the paper and/or the Supplementary Materials. The Sr/Ca geochemical data for core F14 used in this study can be accessed through the online repository NOAA/World Data Service for Paleoclimatology (https://www.ncei.noaa.gov/access/paleo-search/study/39439). CMIP6 data used in this study can be obtained from the Earth Systems Grid Federation website (https://esgf-node.llnl.gov/projects/cmip6/).

Submitted 5 February 2024
Accepted 10 July 2024
Published 14 August 2024
10.1126/sciadv.ado5107